Modelling and simulation on a novel meat grinder circuit for the dynamic pulsed power load

Wenyi Ye[1,3], Weidong Xu[1,2], Rongyao Fu[1,2], Rong Xu[1,2], Zunjing Fu[1,3], Wen Tian[1,3], Dongdong Zhang[4*] and Ping Yan[1,2]

[1]Institute of Electrical Engineering, Chinese Academy of Sciences, Beijing 100190, China
[2]Key Laboratory of Power Electronics and Electric Drive, Chinese Academy of Science, Beijing 100190, China
[3]University of Chinese Academy of Science, Beijing 100049, China
[4]Dalian University of Technology, Dalian 116024, Liaoning, China

Abstract. Compared with the capacitive pulsed power supply (CPPS), the inductive pulsed power supply (IPPS) is considered to have broader prospects because of its theoretically higher energy densities. Most recent researches focus on characteristics of the IPPS with a fixed load, which is rather different from practical applications from the engineering point of view. In this paper, with the purpose of preliminarily verifying the IPPS's feasibility, the performance of the novel meat grinder circuit with a dynamic load model is presented and analysed under PSpice environment. The analysis model is based on the parameters of the four-module IPPS and the pulsed power load built in Institute of Electrical Engineering. Finally, the comparison between the IPPS and the CPPS with same initial energy is carried out.

1 Introduction

The pulsed power supply (PPS) requires power in giga-watt range and mega-ampere currents which should be maintained for several milliseconds [1-3]. Because of higher energy densities, the inductive pulsed power supply (IPPS) attracts interest [4,5].

Researches on derived circuits of two basic topologies, the XRAM and the meat grinder, last for years [6-8]. In terms of the meat grinder, the Slow TRansfer of Energy Through Capacitive Hybrid (STRETCH) meat grinder is proposed by Institute for Advanced Technology [9,10]. Besides, both STRETCH meat grinder with SECT and STRETCH meat grinder with ICCOS are developed by Tsinghua University [11,12].

As shown in Fig. 1, a novel meat grinder circuit is proposed by Institute of Electrical Engineering (IEE) [13].

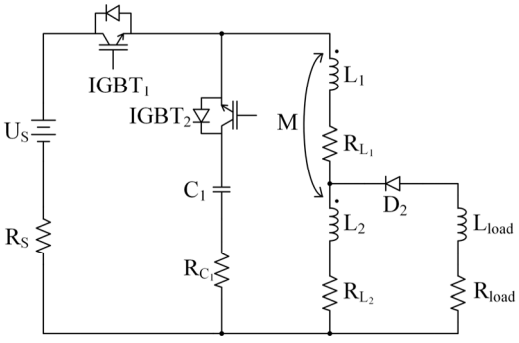

Fig. 1. Topology of the novel meat grinder

Compared with STRETCH meat grinder, the main switches are replaced by IGBTs in order to obtain better load current waveforms and lower voltage stress on the opening switch. Note that the direction of diode in the parallel of $IGBT_2$ is opposite to the diode with the same position in the STRETCH meat grinder circuit.

The IPPS designed by IEE comprises four novel meat grinder modules. With a fixed 0.4-mΩ resistance, the experimental load current reached 30.40 kA with a 1.7-ms pulse width, which basically meets the requirement of a small-scale pulse high-current launcher.

Fig. 2. The Four-module IPPS in IEE

In this paper, the mathematical model of the pulse high-current launcher is presented, and the dynamic load model including the velocity and displacement of the armature is used to replace the fixed load under PSpice environment. The efficiency of the system consisting of the four-module IPPS and the pulse high-current launcher is calculated. The comparison between the IPPS and the CPPS with same initial energy is carried out in

* Corresponding author: zhdd80@dlut.edu.cn

order to reveal any further research possibilities for its improvements.

2 Establishment of dynamic model for the pulse high-current launcher

As shown in Fig. 3(a), the structure of one kind of the pulse high-current launcher consists of four parallel rails and a sliding armature. The process of launching is the interaction of multiple physical fields. As shown in Fig. 3 (b), the electrical equivalent model is established to describe its complex physical phenomena.

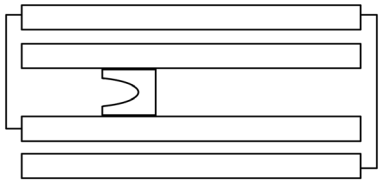

(a) The structure of the pulse high-current launcher

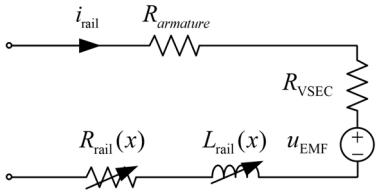

(b) The equivalent model of the pulse high-current launcher

Fig. 3. The structure and equivalent circuit of the launcher

2.1. Rail inductance and resistance

The inductance of the rail $L_{\text{rail}}(x)$ and the resistance of the rail $R_{\text{rail}}(x)$ increase linearly by the displacement of the armature. Both of them are given by

$$L_{\text{rail}}(x) = L_0 + L^{'}x \tag{1}$$

$$R_{\text{rail}}(x) = R_0 + R^{'}x \tag{2}$$

where x is the displacement of the armature, $L^{'}$ and $R^{'}$ are inductance gradient and resistance gradient of the rail respectively, L_0 and R_0 are initial inductance and resistance of the rail respectively.

2.2. Contact velocity skin effect

During the process of launching, contact and interface physics must be considered because of its great impact on the loss of system energy. Based on the theory of contact velocity skin effect (VSEC), this performance-limiting effect represents as an equivalent resistance R_{VSEC} [14]. The equivalent resistance R_{VSEC} is given by

$$R_{\text{VSEC}} = \text{R}_{\text{VC}} \cdot v^{1.5} \tag{3}$$

where R_{VC} is the proportional coefficient, v is the velocity of the armature.

2.3. Back-electromotive force

The motion of armature causes the back-electromotive force u_{EMF}, which is given by

$$u_{\text{EMF}} = L^{'}v i_{\text{rail}} \tag{4}$$

where i_{rail} is the current flowing through the rail.

2.4. Friction force

In the practical situation, the contact pressure F_{C} at the rail-armature interface consists of the mechanical stress F_{Cmech} and the electromagnetic force F_{Cem}. As the current rises, the electromagnetic force F_{Cem} becomes an overwhelming force over the contact pressure F_{C}. The contact pressure F_{C} and a simplified friction force f are given by

$$F_{\text{Cem}} = \frac{l_{\text{wing}} L^{'}}{3s} i_{\text{rail}}^2 \tag{5}$$

$$f = \mu_2 F_C \approx \mu_2 F_{\text{Cem}} \tag{6}$$

where l_{wing} is the length of the armature's wing, s is the distance between inner rails, and μ_2 is the friction coefficient.

2.5. Calculation module for the velocity and displacement of the armature

The driving force generated in the armature and the acceleration of the armature are given by

$$F_{\text{EM}} = \frac{L^{'}}{2} i_{\text{rail}}^2 \tag{7}$$

$$a = \frac{F_{\text{EM}} - f}{m} = \frac{3s - 2\mu_2 l_{\text{wing}}}{6ms} L^{'} i_{\text{rail}}^2 \tag{8}$$

where m is the mass of the armature, l_{wing} is the length of the armature's wing.

Compared with the acceleration of the armature without considering the friction force, the equivalent inductance gradient $L_{eq}^{'}$ is given by

$$L_{eq}^{'} = \frac{3s - 2\mu_2 l_{\text{wing}}}{3s} L^{'} \tag{9}$$

The velocity of the armature is given by

$$v(t) = v_0 + \frac{L_{eq}^{'}}{2m} \int_0^t i_{rail}^2(\tau)\, d\tau \tag{10}$$

Suppose that $u_L(t)$, the voltage the inductor L_{cal}, is given by

$$u_L(t) = i_{rail}^2(t) \tag{11}$$

and $i_L(t)$, the current of the inductor L_{cal}, is given by

$$i_L(t) = i_0 + \frac{1}{L_{cal}}\int_0^t u_L(\tau)d\tau = i_0 + \frac{1}{L_{cal}}\int_0^t i_{rail}^2(\tau)d\tau \tag{12}$$

where i_0 is the initial current of the inductor L_{cal}.

With the definition of $L_{cal}=2m/L_{eq}^{'}$ and $i_0 = v_0$, (10) and (12) are consistent, which means $i_L(t)$ represents the velocity of the armature.

Based on the above analysis, the calculation module for the velocity and displacement of the armature is presented in Fig. 4.

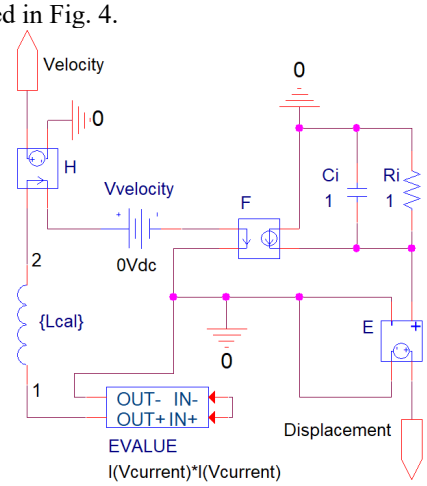

Fig. 4. The calculation module for the dynamic load

As shown in Fig. 4, the voltage across the inductor depends on the EVALUE part which works as a voltage source with the output of i_{rail}^2. The displacement of the armature is obtained by the integration of the current through the inductor.

3 Performance of the novel meat grinder with the pulse high-current launcher

Most discharge characteristics of derived meat grinder circuits have two current peaks. In order to realize a large scale IPPS system to meet the requirement from the engineering point of view, a novel meat grinder is proposed [13].

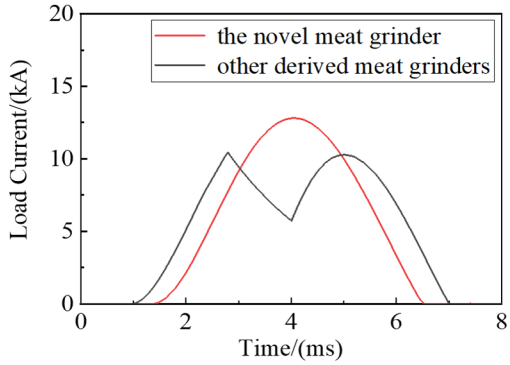

Fig. 5. Typical load currents of the novel meat grinder and other derived meat grinders

As shown in Fig. 5, both the novel meat grinder and the STRETCH meat grinder in the simulation use same parameters of the four-module IPPS with the fixed load of a 0.4-mΩ resistance and a 1-μH inductor. From the results of simulation and experiment, the novel meat grinder circuit has better load currents waveforms and higher peak current, which means it is more easily to be shaped for superposition.

The parameters of the four-module IPPS and the pulse high-current launcher is presented in Table 1.

It is noteworthy that the operation of IGBTs affects the performance of the novel meat grinder circuit. The principle is that the conduction of $IGBT_2$ must precede the turn-off of $IGBT_1$. Otherwise the delay of conduction on $IGBT_2$ leads to higher voltage stress on the opening switch $IGBT_1$. In this paper, the operation of IGBTs is as the same as the operation in the experiment with a 0.4-mΩ resistance. Namely, the turn-on of $IGBT_2$ is 0.2-ms earlier than the turn-off of $IGBT_1$, and t_L, the pre-charge time of the primary inductor L_1 and the secondary inductor L_2, is 12.2 ms.

Table 1. Parameters of the IPPS and the launcher.

Symbol	Description	value
C_S	primary capacitor	76 mF
C_1	energy transfer capacitor	1.6 mF
t_C	pre-charged time of capacitors	5 ms
L_1	inductance of primary inductor	1150 μH
R_1	resistance of primary inductor	83 mΩ
L_2	inductance of secondary inductor	3 μH
R_2	resistance of secondary inductor	0.75 mΩ
k	coupling factor	0.75
t_L	pre-charged time of inductors	12.2 ms
$L^{'}$	inductance gradient of the rail	0.9 μH/m
$R^{'}$	resistance gradient of the rail	0.2 mΩ/m
L_0	initial inductance of the rail	1.5 μH
R_0	initial resistance of the rail	0.38 mΩ
R_{VC}	proportional coefficient	6×10^{-9}
μ_2	friction coefficient	0.08
m	mass of the armature	15 g
s	distance between the rail	23 mm
l_{wing}	length of the armature's wing	8.67 mm

To achieve a higher current peak, four modules of the novel meat grinder are triggered simultaneously. As shown in Fig. 6, the performance of the four-module IPPS including the voltage of the primary capacitor C_S and the energy transfer capacitor C_1, the current through the inductors L_1 and L_2, the current through the rail, the velocity and the displacement of the armature is presented.

According to the simulation, the pre-charge voltage of C_S and C_1 in each module reach 662.021 V and 682.249 V, respectively. The pre-charge current of the inductors in each module reach 3.286 kA, which is symbolized as I_0. During the launching, the load current reaches the peak of 82.807-kA at 21.638 ms. Considering that the length of the launcher is 2.4 m, the muzzle time is at 27.059 ms and the process of the launching which starts with the discharge of the inductors lasts 8.859 ms. The muzzle velocity is 450.570 m/s with the 15-g armature. The residual voltage of C_S and C_1 in each module are 320.923 V and 1798.2 V, respectively.

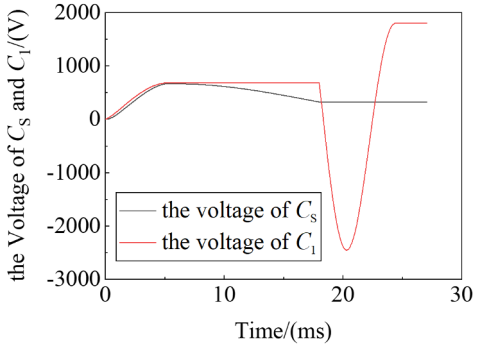

(a) The Voltage of C_S and C_1

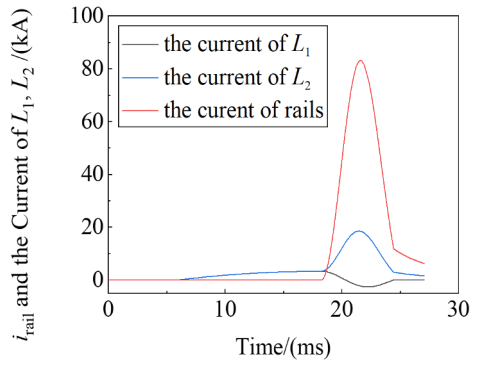

(b) Load current and the current of L_1 and L_2

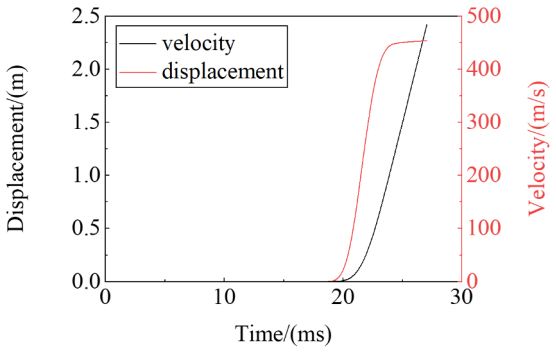

(c) The velocity and displacement of the Armature

Fig. 6. Performance of the Four-Module IPPS with the Pulse High-Current Launcher

According to the simulation, the initial energy of IPPS system is given by

$$W_0 = 4\times\left(\frac{1}{2}C_S U_{C_S}^2 + \frac{1}{2}C_1 U_{C_1}^2\right) = 68.107 \text{ kJ} \quad (13)$$

The energy of charging to the inductors L_1 and L_2 is given by

$$W_L = 4\times\left[\frac{1}{2}(L_1 + L_2)I_0^2\right] = 24.900 \text{ kJ} \quad (14)$$

The efficiency of charging is given by

$$\eta_1 = \frac{W_L}{W_0} = 36.560\ \% \quad (15)$$

The muzzle energy is given by

$$W_k = \frac{1}{2}mv^2 = 1.523 \text{ kJ} \quad (16)$$

The efficiency of discharging and the whole system are given by

$$\eta_2 = \frac{W_k}{W_L} = 6.115\ \% \quad (17)$$

$$\eta = \eta_1 \cdot \eta_2 = 2.236\ \% \quad (18)$$

4 Comparison between the IPPS and the CPPS

From the engineering point of view for pulse high-current launchers, the novel meat grinder, or other PPSs, must drive the projectile at rather higher muzzle velocity than the projectile launched by gas dynamic launchers. Unfortunately, the IPPS with mature technologies has not been developed up to now. Meanwhile, the CPPS has proven its reliability and usability in most researches [2, 4,15]. Therefore, it is necessary to draw a comparison between the novel meat grinder circuit and the CPPS. The simulation and analysis in this paper is the basis for improvements and the definite construction for full-scale demonstration.

In order to access the performance of the IPPS and reveal further possibilities for its improvements, the CPPS with same initial primary energy is simulated as well. The parameters of the CPPS in IEE is shown in Table 2.

Table 2. Parameters of the PFU in the CPPS.

Symbol	Description	value
C	capacitance of pulse capacitor	2.03 mF
R_C	resistance of pulse capacitor	1.70 mΩ
U_0	pre-charged voltage of C	1495.6 V
L	inductance of pulse forming inductor	13.28 μH
R_L	resistance of pulse forming inductor	2.81 mΩ
n	number of PFU	30

Considering that the IPPS is trigged simultaneously, the triggering method of the CPPS is the same. The

comparison between the IPPS and the CPPS is shown in Table 3.

Table 3. Comparison between the IPPS and the CPPS.

Performance	IPPS	CPPS
initial energy/(kJ)	68.107	68.107
triggering method	synchronous triggering	synchronous triggering
load current peak/(kA)	82.807	210.035
muzzle velocity/(m/s)	450.570	1043.472
muzzle energy/(kJ)	1.523	8.166
system efficiency/(%)	2.236	11.990

According to the comparison, the efficiency of the CPPS is 5.36 times higher than the efficiency of the IPPS.

Note that the capacitors C_S and C_1 store a certain mount of energy after launching. The residual energy of the capacitors C_S in the IPPS is 15.655 kJ, which is 22.986 % of the initial energy. The residual energy of the capacitors C_S in the IPPS is 10.347 kJ, which is 15.192 % of the initial energy. Both of them comprise a considerable propotion of the initial energy, which means great potential for efficiency improvement. Further researches would be needed for any feasibilities, methods and actual ratio for the muzzle energy of the residual energy recovery.

5 Conclusion

With the purpose of verifying the feasibility of the IPPS and revealing its further improvement, the dynamic model for the pulse high-current launcher is established in this paper. Based on the practical parameters of the novel meat grinder circuit and the launcher built by IEE, the performance of the four-module IPPS is simulated and analysed.

With the initial energy of 68.107 kJ, the muzzle velocity and the muzzle energy are 450.570 m/s and 1.523 kJ, respectively. According to the calculation, the efficiency of charging and discharging are 36.560 % and 6.115 %, respectively. The system efficiency of the IPPS is 2.236 %, which is much lower than the CPPS with same initial energy. The reason of low efficiency in the IPPS is a considerable amount of residual energy stored in the primary capacitor C_S and the energy transfer capacitor C_1. Further researches will focus on the residual energy recovery to improve the efficiency of the IPPS.

References

1. I. R. McNab. Large-scale pulsed power oppotunities and chanllenges, IEEE Trans. Plasma Sci. **42**, 5, 1118-1127 (2014)
2. I. R. McNab, Pulsed power options for large EM launchers, IEEE Trans. Plasma Sci. **43**, 5, 1352-1357 (2015)
3. O. Liebfrid, Review of inductive pulsed power generators for railgun, IEEE Trans. Plasma Sci. **45**, 7, 1108-1114 (2017)
4. O. Liebfried, S. Hundertmark, P. Frings, Inductive pulsed power supply for a railgun artillery system, IEEE Trans. Plasma Sci. **47**, 5, 2550-2555 (2019)
5. X. Yu, X Liu, Review of the meat grinder circuits for railgun, IEEE Trans. Plasma Sci. **45**, 7, 1086-1094 (2017)
6. O. Zucker, J. Wyatt, K. Lindner, The meat grinder: theoretical and practical limitations, IEEE Trans. Magn. **20**, 2, 391-394 (1984)
7. O. Liebfried, V. Brommer, A four-stage XRAM generator as inductive pulsed power supply for a small-caliber railgun, IEEE Trans. Plasma Sci. **41**, 10, 2805-2809 (2013)
8. H. Sun, X. Yu, B. Li, et al., Meat grinder with ACC circuit: a novel circuit for inductive pulsed power supplies, IEEE Trans. Plasma Sci. **48**, 2, 566-570 (2020)
9. A. Sitzman, D. Surls, J. Mallick, Stretch meat grinder: a novel circuit topology for reducing opening switch voltage stress, *2005 IEEE Pulsed Power Conference*, Monterey, CA, 493-496 (2005)
10. A. Sitzman, D. Surls, J. Mallick, Design, construction, and testing of an inductive pulsed-power supply for a small railgun, IEEE Trans. Magn. **43**, 1, 270-274 (2007)
11. X. Yu, R. Ban, X. Liu, et al., The meat grinder with SECT circuit, IEEE Trans. Plasma Sci, **45**, 7, 1448-1452 (2017)
12. X. Yu, X. Chu, STRETCH meat grinder with ICCOS, IEEE Trans. Plasma Sci, **41**, 5, 1346-1351 (2013)
13. Y. Wang, D. Zhang, R. Fu, et al., Design of a high current inductive pulsed power supply with millisecong pulse width, Trans. China Electrotech. Soc., **35**, 23, 5025-5030 (2020)
14. T. Engel, J. Neri, M. Veracka., Characterization of the velocity skin effect in the surface layer of a railgun sliding contact, IEEE Trans. Magn. **44**, 7, 1837-1844 (2008)
15. S. Hundertmark, O. Liebfried, Options for an electric launcher system, IEEE Trans. Plasma Sci. **47**, 10, 4433-4438 (2019)